Photocatalytic CO_2 reduction and environmental remediation using mineralization of toxic metal cations products

Tianyi Lai,†[a] Jikang Wang, †[a] Wenbo Xiong,†[a] Huijuan Wang,[a] Mufei Yang,[a] Tian Li,[a] Xianggui Kong,[a] Xiaoxin Zou,[b] Yufei Zhao,*[a] Dermot O'Hare[c] and Yu-Fei Song*[a]

[a]State Key Laboratory of Chemical Resource Engineering, Beijing Advanced Innovation Center for Soft Matter Science and Engineering, Beijing University of Chemical Technology, Beijing 100029, China.

[b]State Key Laboratory of Inorganic Synthesis and Preparative Chemistry College of Chemistry, Jilin University, Changchun 130012, China.

[c]Chemistry Research Laboratory, Department of Chemistry, University of Oxford, Mansfield Road, Oxford OX1 3TA, United Kingdom.

* Corresponding author.

Email: zhaoyufei@mail.buct.edu.cn; songyf@mail.buct.edu.cn.

† These authors contributed equally to this work.

Abstract: Exploring a sustainable route for the efficient treating/recycling of heavy metal (like Ni^{2+}, Cd^{2+}, Cu^{2+}) contamination of water is highly desirable both from the environment and resource view. Herein, we reported the scale-up synthesis of monolayer magnesium-aluminium layered double hydroxide (m-MgAl-LDH) nanosheets, which showed exceptional ability to mineralize Ni^{2+}, Cd^{2+} and Cu^{2+} rapidly and efficiently. Furthermore, m-MgAl-LDH can purify 1 ppm Cu^{2+}, Ni^{2+} and Cd^{2+} to

safe levels. The sorption sites of heavy metal ions were revealed. Ni^{2+} and Cd^{2+} substitute for the Mg^{2+} sites within the MgAl-LDH layers, while Cu^{2+} ions anchor on the surface of MgAl-LDH with high dispersion. The mineralized products from Ni^{2+} and Cu^{2+} cations further showed excellent performance in visible-light-induced photocatalytic reduction of CO_2 and removal of anions (like PO_4^{3-} and toxic AsO_2^- ions) efficiently, providing an alternative for the mitigation of energy and resource crisis.

Keywords: heavy metals, photocatalysis, mineralization, layered double hydroxides

1. Introduction

Heavy metal pollution (such as Ni^{2+}, Cd^{2+} and Cu^{2+}) in industrial wastewater and soil, one of the most severe and detrimental contamination problems, is produced by the metallurgy, mining, and electroplating industries.(Guo et al., 2021; Krstić et al., 2018; Szczepaniak et al., 2020) Heavy metals often possess high toxicity and can easily be accumulated through the food chain, exerting a significant threat to the existence of life.(Gore et al., 2016; Guan et al., 2018; Li et al., 2020; Xu et al., 2017) The *in situ* immobilization methods, which use stabilizers through toxic element adsorption and precipitation processes, have been considered promising methods for large-scale wastewater treatment. They provide ideal removal efficiency in an economical and environmentally friendly way(Bilal et al., 2013; Shan et al., 2015) and are usually preferable to other traditional remediation methods, such as chemical precipitation,(Zhou et al., 2018) ion exchange(Lam et al., 2018) and membrane filtration.(Vital et al., 2018) Currently, a range of stabilizers/adsorbents, including biochar, clay minerals, and other organic and inorganic materials, have been developed.(Egene et al., 2018;

Feizi et al., 2019; He et al., 2019; He et al., 2020; Hoang et al., 2020; Wang et al., 2017a; Yu et al., 2017a) However, their removal rate and capability are still unsatisfactory to meet the commercial requirements. The precise location of the adsorption sites for metal ions is still often ambiguous, which significantly hinders the rational design and development of effective stabilizers. Furthermore, with the increasingly severe crisis of energy and resources, more attention should be paid to the recovery and utilization of resources, like Ni and Cu.

For the mentioned reasons, developing a new kind of heavy metal capturer that can meet the development of practical use is vital. Layered double hydroxides (LDHs), which has the general formula as $[(M^{z+}_{1-x}M'^{y+}_{x}(OH)_2)]^{w+}(A^{n-})_{w/n}\cdot mH_2O]$, offers a range of possibilities for pollution remediation as they offer cation and anion tunability, relatively larger specific surface areas and flexible platelet thickness.(Jin et al., 2020; Wang and O'Hare, 2012; Zhang et al., 2020) Through intercalating anionic guests into LDH gallery, the LDH hybrid structures have been used to efficiently treat heavy metal pollution using S_x^{2-} or MoS_4^{2-}intercalated MgAl-LDH.(Ma et al., 2017; Shi et al., 2020) Recently, it was reported that CaAl-LDH could be used as an efficient stabilizer to remove Cd^{2+} through an isomorphous substitution process, forming a super-stable mineralization structure (SSMS) CdAl-LDH with an ultrasmall K_{sp} value of 10^{-48}, 20 orders of magnitudes smaller than that of CaAl-LDH (K_{sp} = ~10^{-28}), similar NiFe-LDH SSMS can also be obtained from CaFe-LDH when treating Ni^{2+} ions.(Haoyuan et al., 2021; Kong et al., 2021) However, traditionally synthesized multilayers LDHs platelet particles cannot achieve ideal treatment performance because the nature of the stacked layers often results in limited exposure of the active mineralization sites. Therefore, the exfoliation of

LDH platelet particles into monolayers may offer an efficient and practical solution for improving the capture performance due to the significantly increased specific surface area and the introduction of coordinatively unsaturated sites.(Chen et al., 2020; Kim et al., 2021; Song and Hu, 2014; Wang et al., 2017b; Yu et al., 2015; Zhao et al., 2016) From the industrial viewpoint, the traditional synthesis of monolayer LDHs using the exfoliation/bottom-up method suffers from many disadvantages such as prolonged time consumption, low yields and inability to isolate solid samples. Separate nucleation and aging steps (SNAS) developed by Duan *et al.* has been commercially used to synthesize nanostructured LDH powders in several successful pilot plants by introducing a colloid mill in the synthesis process LDHs.(Evans and Duan, 2006; Kuai et al., 2019) LDH powders have been commercially developed for use as ultraviolet-absorbents,(Feng et al., 2006) infrared-absorbents,(Wang et al., 2010) flame retardants(Liu et al., 2021; Xu et al., 2012), and sorbents.(Li et al., 2016; Sajid and Basheer, 2016) Recently, we found that the SNAS strategy can be used to produce dispersions of monolayer LDHs using NH_4OH(aq) (Chi et al., 2020) or by adding formamide.(Bai et al., 2021) However, the LDH monolayers spontaneously restack into the more favored bulk platelet structure during the drying process. This arises from the strong electrostatic and hydrogen bonding interactions between the LDH monolayers. Thus the efficient large-scale synthesis of monolayer dispersed LDH powders samples for industrial application in the remediation of heavy metal ions is of great importance and is still a challenging unmet need.(Hu et al., 2019; Wang and O'Hare, 2013; Yu et al., 2017b)

O’Hare *et al.* has reported an efficient approach to synthesizing monolayer LDH powders using the aqueous miscible organic solvent treatment (AMOST) method, the first scalable and straightforward method to produce monolayer LDH powder samples.(Funnell et al., 2014; Wang and O'Hare, 2013) Herein, we have combined the SNAS and AMOST methods to successfully produce a scalable approach to synthesizing monolayer LDH powders (Scheme 1). The as-synthesized monolayer MgAl-LDH (denoted as m-MgAl-LDH) exhibited an extremely efficient capture capacity of more than ~99% from 100 ppm Cu^{2+}, Ni^{2+} and Cd^{2+}, respectively. The capture performance at low cation concentrations (1 ppm) was also prominent. Furthermore, the successful application of mineralized products in photocatalytic CO_2 reduction and removal anions (like PO_4^{3-} and toxic AsO_2^- ions), provides a green solution to alleviate the resource and energy crisis. We believe this study can provide a practical approach for the development of efficient capture and recycling of heavy metal ions through the formation of SSMS.

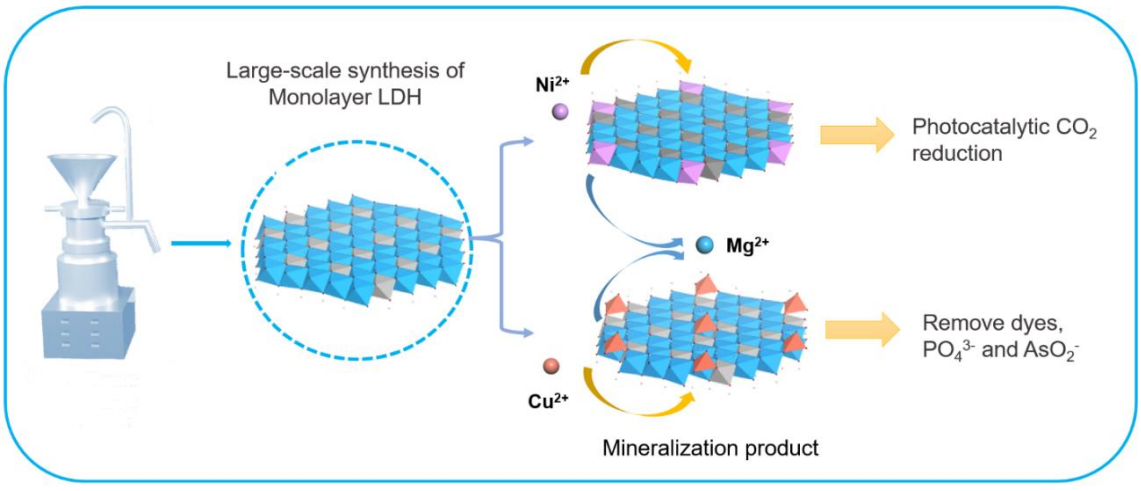

Scheme 1. Schematic illustration of the efficient synthesis of monolayer LDH nanosheet powders for the heavy metal cation mineralization and the utilization in photocatalytic CO_2 reduction, removal dye, PO_4^{3-} and toxic AsO_2^-, etc.

2. Experimental section

2.1 Synthetic procedures

Synthesis of monolayer Mg_3Al-LDH nanosheets (m-MgAl-LDH). In a typical synthesis, 0.01875 mol $Mg(NO_3)_2 \cdot 6H_2O$ (4.81g) and 0.00625 mol $Al(NO_3)_3 \cdot 9H_2O$ (2.34g) accompanied with 0.0625 mol H_3BO_3 (3.88g) were dissolved in deionized water, denoted as solution A. 0.075 mol of NaOH (3.0g) was also dissolved in deionized water which denoted as solution B. Solution A and B were simultaneously added to the colloid mill (Figure S1) at a constant pouring speed keeping the rotation speed at 3000 rpm. After stirring for 2 min, the wet cake product was collected by centrifugation, washed with acetone three or four times until neutral pH, followed by drying in a vacuum oven to yield m-MgAl-LDH ($[Mg_{0.75}Al_{0.25}(OH)_2](B_4O_5(OH)_4])_{0.125} \cdot 0.5H_2O$).

Synthesis of multilayer Mg_3Al-LDH nanosheets (u-MgAl-LDH). A sample of an equivalent multilayer $[Mg_{0.75}Al_{0.25}(OH)_2](B_4O_5(OH)_4])_{0.125} \cdot 0.5H_2O$ (u-MgAl-LDH) was prepared by the same procedure except the final wet cake was dispersed in water rather than acetone (without AMOST).

Pretreatment of m-MgAl-LDH for treating actual electroplating wastewater. m-MgAl-LDH was put into the muffle furnace under air circumstance at 300°C

for 240 minutes with heating rate of 10 ^{o}C min^{-1} for adsorbing actual Ni, Cu - containing electroplating liquid (from AVIC Beijing Keeven Aviation Instrument Co., Ltd.).

2.2 Characterization, capture for heavy metal ions, kinetic and isotherm studies, photocatalytic test, and anions adsorption experiment can be found in SI.

3. Results and discussion

3.1 Morphology and structure of MgAl-LDH

Figure 1a showed the X-ray diffraction (XRD) data for m-MgAl-LDH. The absence of (*00l*) Bragg diffraction features indicated no long-range platelet stacking in this sample.(Song and Hu, 2014; Wang et al., 2018) Dispersing m-MgAl-LDH in water caused the stacking of monolayers, forming the multilayer MgAl-LDH (denoted as u-MgAl-LDH). However, the XRD data (Figure 1a) from the u-MgAl-LDH showed weak and broad Bragg diffraction peaks that may be indexed as (*00l*) reflections due to the restacking of LDH nanosheets. This indicated that the sample consisted of multilayer LDH nanosheets. The observed interlayer separation of u-MgAl-LDH was 9.7 Å, consistent with the intercalation of the tetraborate ($[B_4O_5(OH)_4]^{2-}$) anion in the interlayer galleries.(Miao et al., 2021)

The Fourier transform infrared (FT-IR) spectra of m-MgAl-LDH and u-MgAl-LDH were shown in Figure 1b. The spectra provided evidence for vibrations arising from the charge balancing borate anions. Both m-MgAl-LDH and u-MgAl-LDH showed vibration bands at 1387, 1022, and 673 cm^{-1} corresponding to $\nu_{as(B3-O)}$, $\nu_{as(B4-O)}$, and $\nu_{a(B4-O)}$ stretching vibrations that may be assigned to the

tetraborate ($[B_4O_5(OH)_4]^{2-}$) anion. As shown in Figure 1c, $[B_4O_5(OH)_4]^{2-}$ were adsorbed onto the surface of m-MgAl-LDH to balance the charge.(Lan et al., 2014) The high-resolution transmission electron microscopy (HRTEM) images (Figure 1d, 1e, S2a, and S2b) and the atomic force microscope (AFM) image (Figure 1f) of m-MgAl-LDH revealed a sheet-like structure with a thickness of about 0.99 nm. From Figure S3, we can see the coexistence and uniform distribution of Mg, Al, O, and B elememts in m-MgAl-LDH. After re-dispersing in water, m-MgAl-LDH was stacked and exhibited the characteristic diffraction peak of multilayer LDH (Figure 1a), and the obtained u-MgAl-LDH sample was ultrathin with a thickness of about 3 nm, corresponding to 3–4 LDH layers, as illustrated in Figure 1g-i and Figure S4. To sum up, we successfully synthesized monolayer m-MgAl-LDH and multilayer u-MgAl-LDH through the SNAS process, and their removal properties will be discussed as follows.

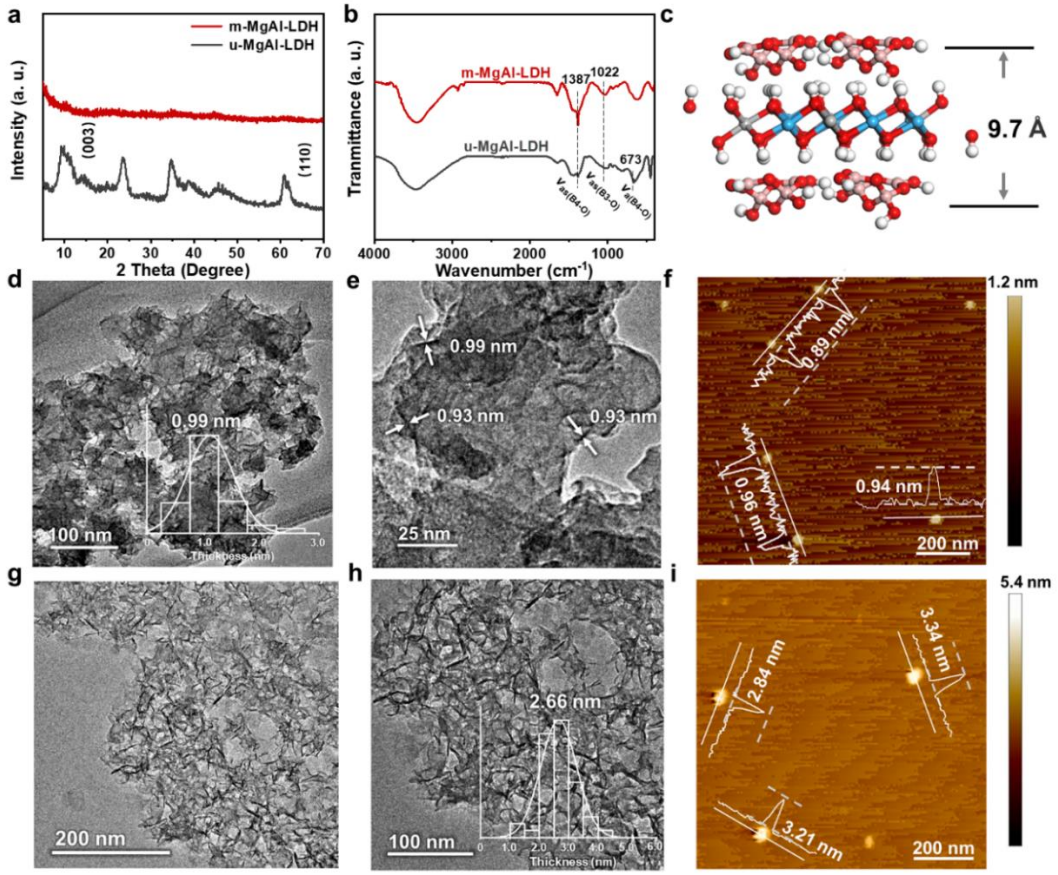

Figure 1. (a) XRD patterns of m-MgAl-LDH and u-MgAl-LDH, (b) FT-IR spectra of m-MgAl-LDH and u-MgAl-LDH, (c) schematic structure of the m-MgAl-LDH, (d, e) HRTEM images of m-MgAl-LDH; (f) AFM image of m-MgAl-LDH, (g, h) HRTEM images of u-MgAl-LDH, (i) AFM image of u-MgAl-LDH.

N_2 Brunauer–Emmett–Teller (BET) adsorption studies were used to determine the specific surface areas of the as-synthesized LDHs. Figure 2a showed m-MgAl-LDH and u-MgAl-LDH had specific surface areas of 294.7 m^2/g and 8.3 m^2/g, respectively. From the pore size distribution of m-MgAl-LDH (Figure 2a inset), it can be seen that most of the pores were mainly mesoporous at about 3.8 nm. Thus, m-MgAl-LDH with a higher surface area may provide a high number of available active sites for heavy metal ion remediation.(Zhao et al., 2020)

3.2 Capture performance of MgAl-LDH for heavy metal ions

We have studied the use of both m-MgAl-LDH and u-MgAl-LDH to capture Ni^{2+} ions from an aqueous solution. In a typical experiment, 40 mg of either m-MgAl-LDH or u-MgAl-LDH was dispersed in 40 mL water containing 100 ppm of Ni^{2+}. The mixture was stirred under 750 rpm for different periods, after which quantitative analysis for the metal ions remaining in the aqueous solution was performed using ICP-OES or ICP-MS. Figure 2b showed the time dependence of the uptake of Ni^{2+} by m-MgAl-LDH and u-MgAl-LDH. m-MgAl-LDH displayed excellent Ni^{2+} capture performance, removing 99.76% Ni^{2+} ions in approx. 20 minutes, giving the final concentration of 0.244 ppm. This performance was much superior to u-MgAl-LDH, which showed merely 7.67% capture efficiency after a contact time of 180 minutes. As shown in Figure S5, HRTEM images demonstrated that the m-MgAl-LDH and u-MgAl-LDH adsorbents after capturing Ni^{2+} still had sheet morphology. The kinetics of Ni^{2+} capture was investigated by fitting this updated data to both the Lagergren's pseudo-first-order and Ho's pseudo-second-order models. The best agreement for both materials was obtained from least-squares fits to Ho's pseudo-second-order model (Figure S6, Table S1). Isotherm fitting results for Ni^{2+} demonstrated that both the removal process of these two samples can be ascribed to Langmuir isotherm model (Figure S7, Table S2). According to the fitting results, q_m for m-MgAl-LDH was 229.89 mg g^{-1}, while for u-MgAl-LDH, it was only 29.36 mg g^{-1}. The remediation performance for Ni^{2+} at low concentration was also investigated (Table 1), m-MgAl-LDH was able to reduce the 1 ppm solution to

the trace level of 0.006 ppm, while the u-MgAl-LDH can only lower the concentration to 0.029 ppm. For actual electroplating liquid (from AVIC Beijing Keeven Aviation Instrument Co., Ltd.) with a much higher Ni^{2+} concentration (7661 ppm) and some Zn^{2+} ions, adding 50 g/L of m-MgAl-LDH can lower the concentration final to 0.050 ppm (Table 2, Figure S8).

Besides, the use of both m-MgAl-LDH and u-MgAl-LDH to capture Cd^{2+} was also studied from an aqueous solution containing 100 ppm Cd^{2+} since the toxic property of Cd^{2+} both in water and soil. m-MgAl-LDH exhibited a 99.41% removal efficiency after 180 minutes, producing a final concentration of 0.594 ppm. In contrast, u-MgAl-LDH exhibited a removal efficiency of only 31.68% with a final concentration of 68.32 ppm (Figure 2c). Similar to both Cu^{2+} and Ni^{2+} removal process, this process can be best fitted to Ho's pseudo-second-order model (Figure S9, Table S3). Isotherm studies also showed a better fitting result with Langmuir isotherm model. The theoretical capacity of m-MgAl-LDH and u-MgAl-LDH was 239.41 mg g^{-1} and 69.74 mg g^{-1}, respectively (Figure S10, Table S4). The standard of Cd^{2+} guideline in drinking water by World Health Organization (WHO)(2010) is 3 ppb, and by using m-MgAl-LDH to treat 1 ppm Cd^{2+} ion, the concentration of Cd^{2+} can be reduced to 2 ppb, which cannot be achieved by u-MgAl-LDH (38 ppb). Therefore, m-MgAl-LDH offers the possibility for remediation of heavy metal polluted water (Table 1).

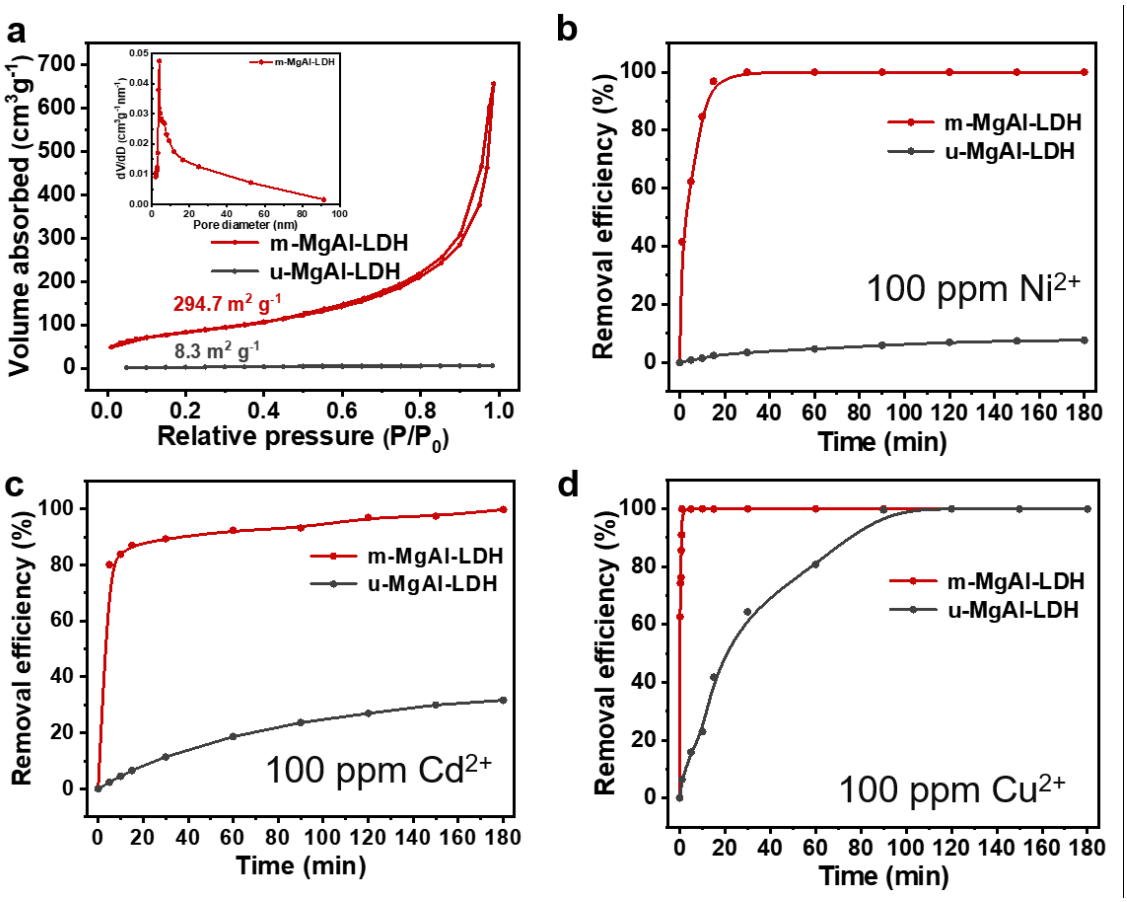

Figure 2. (a) N_2 BET adsorption-desorption isotherms for m-MgAl-LDH and u-MgAl-LDH and pore size distribution of m-MgAl-LDH (inset), time dependence for (b) Ni^{2+} (c) Cd^{2+} and (d) Cu^{2+}, sorption efficiency for m-MgAl-LDH and u-MgAl-LDH (initial Ni^{2+}, Cd^{2+}, Cu^{2+}concentration = 100 ppm, respectively, pH = 5, temperature = 303 K, adsorbent dosage = 1 g L^{-1}).

Table 1. Capture performance of m-MgAl-LDH and u-MgAl-LDH for Cu^{2+}, Ni^{2+}, Cd^{2+} containing electroplating waste liquid with the concentrations of 100 ppm and 1 ppm.

Heavy metal ions	Adsorbent	C_0 (ppm)	C_f (ppm)	Removal efficiency (%)
Ni^{2+}	m-MgAl-LDH	100	0.244	99.76
	u-MgAl-LDH		92.33	7.67
	m-MgAl-LDH	1	0.006	99.37
	u-MgAl-LDH		0.029	97.07
Cd^{2+}	m-MgAl-LDH	100	0.594	99.41
	u-MgAl-LDH		68.32	31.68
	m-MgAl-LDH	1	0.002	99.79
	u-MgAl-LDH		0.038	96.14
Cu^{2+}	m-MgAl-LDH	100	0.016	99.98
	u-MgAl-LDH		0.732	99.27
	m-MgAl-LDH	1	0.004	99.59
	u-MgAl-LDH		0.006	99.36

Table 2. Capture performance of m-MgAl-LDH for real Cu and Ni-containing electroplating wastewater (from AVIC Beijing Keeven Aviation Instrument Co., Ltd.).

Real electroplating wastewater	Heavy metal ions	C_0 (ppm)	C_f (ppm)	World Health Organization drinking water standards (ppm)	Removal efficiency (%)
Nickel-containing electroplating wastewater	Ni	7661	0.050	0.070	99.99
	Zn	98	0.010	1.000[a]	99.99
Copper-containing electroplating wastewater	Cu	8343	0.158	2.000	99.99
	Zn	49	0.066	1.000[a]	99.97
	Ni	17	0.002	0.070	99.99

[a] standards for drinking water quality from China

We further studied the use of both m-MgAl-LDH and u-MgAl-LDH to capture Cu^{2+} from an aqueous solution, with the same experiment condition as above. Figure 2d showed the time dependence of the uptake of Cu^{2+}. We can see that m-MgAl-LDH exhibited a much more rapid Cu^{2+} capture response with an ultimate uptake efficiency of 99.98% after only 1 minute of contact time, giving the final Cu concentration of 0.016 ppm. In contrast, the u-MgAl-LDH took 90 minutes to attain the capture efficiency of 99.27%, resulting in the final Cu^{2+} concentration of 0.732 ppm, much longer than that of m-MgAl-LDH. For both m-MgAl-LDH and u-MgAl-LDH, the Cu^{2+} capture process (Figure S11a) results

in a shift of the (003) Bragg reflection that can be ascribed to the anion-exchange of the intercalated $[B_4O_5(OH)_4]^{2-}$ anions. According to the FT-IR results in Figure S11b, the products after capture are proved to be intercalated by both NO_3^- and borate anions. HRTEM images of the products of m-MgAl-LDH and u-MgAl-LDH after capture showed that both samples maintained a sheet-like morphology, while the m-MgAl-LDH (Figure S12a, b) contained both monolayer nanosheets with the thickness of 0.8 nm (consistent with the thickness of monolayer NO_3^- intercalated LDH) and stacked ones with the thickness of 1.7 nm. As for u-MgAl-LDH, HRTEM images showed thicker nanosheets with a thickness of around 5 nm (Figure S12c, d). HRTEM results illustrated that m-MgAl-LDH partially maintained monolayer sheets after the capture process while u-MgAl-LDH showed all stacked nanosheets. After 180 minutes, the specific areas of m-MgAl-LDH and u-MgAl-LDH were determined to be 61.8 m^2/g and 3.4 m^2/g, respectively (Figure S13). The higher specific surface area of m-MgAl-LDH indicates that despite the layers of m-MgAl-LDH restacking during the capture process, it can still provide extensive sites for Cu^{2+} capture.

The rate of Cu^{2+} capture was modelled using Lagergren's pseudo-first-order and Ho's pseudo-second-order models (Figure S14 and Table S5). A correlation coefficient (R^2) of better than 0.99 was obtained for both materials using Ho's pseudo-second-order models. This indicates that Cu^{2+} capture by both m-MgAl-LDH and u-MgAl-LDH is most like chemisorption.(Wang et al., 2016) In particular, for m-MgAl-LDH, the final concentration of 0.016 ppm Cu^{2+} can be reached from an initial 100 ppm Cu^{2+} solution, much lower than achievable by u-MgAl-LDH (0.732 ppm, Table 1). Furthermore, m-MgAl-LDH showed a dramatically increased capture rate, *ca*. 350 times that found for u-MgAl-LDH.

Maximum capture capacity of m-MgAl-LDH and u-MgAl-LDH was determined equilibrium adsorption studies, as shown in Figure S15 and Table S6. The best R^2 was found fitting with the Langmuir isotherm model, suggesting a monolayer adsorption process.(Farrukh et al., 2013) Meanwhile, q_m calculated is 185.87 mg g^{-1} and 182.82 mg g^{-1} for m-MgAl-LDH and u-MgAl-LDH. Studies with much lower Cu^{2+} concentrations (1 ppm) revealed that m-MgAl-LDH also exhibited excellent capture capabilities. For example, m-MgAl-LDH can lower a 1 ppm Cu^{2+} solution to trace levels of 0.004 ppm Cu^{2+} (Table 1), superior to u-MgAl-LDH, further indicating the unique features of the monolayer LDH materials. A further application for actual electroplating waste liquid (with 8343 ppm concentration of Cu^{2+} ions and some Zn^{2+} and Ni^{2+} ions) from AVIC Beijing Keeven Aviation Instrument Co., Ltd. was also shown in Table 2 and Figure S16, m-MgAl-LDH can lower high concentration Cu^{2+} to trace level of 0.158 ppm by adding 50 g/L of m-MgAl-LDH, lower than that of WHO drinking water standard of Cu ion and other Zn and Ni ions, which meant that our material can be used in practical production.

3.3 Mechanism of capturing heavy metal ions by MgAl-LDH

The difference capture rate between m-MgAl-LDH and u-MgAl-LDH toward different ions may be associated with the presence of different chemical binding environments. We first studied the removal of Ni^{2+} using Ni K-edge XANES and EXAFS (Figure 3a). From the XANES spectra, we found that the Ni is adsorbed on MgAl-LDHs in the +2 oxidation. As shown in k-space EXAFS (Figure 3b), both m-MgAl-LDH and u-MgAl-LDH showed distinct oscillations from

$Ni(OH)_2$. For instance, a series of characteristic peaks of $Ni(OH)_2$ at 7.3 $Å^{-1}$, 7.9 $Å^{-1}$, 8.3 $Å^{-1}$, and 9.4 $Å^{-1}$ were significantly shifted compared with m-MgAl-LDH and u-MgAl-LDH, and m-MgAl-LDH and u-MgAl-LDH did not show the characteristic peaks of $Ni(OH)_2$ at 5.7 $Å^{-1}$ and 6.9 $Å^{-1}$. We believed this can be ascribed to a subtle change in the environment of Ni in MgAl-LDHs. The radial distribution function data (Figure 3c) confirmed a similar coordination environment as LDHs, with the first shell (Ni-O) at 1.6 Å and the second shell (Ni-M) at 2.7 Å, this is similar to the model $Ni(OH)_2$ sample. This data suggested Ni^{2+} undergoes cation substitution into the MgAl-LDH layers (Figure 3d).(Kong et al., 2021) Furthermore, we found the leaching Mg^{2+} into the aqueous phase after Ni removal process (Figure S17), while no Al^{3+} was detected in the aqueous phase, thus we can conclude that Ni^{2+} undergoes isomorphous substitution for Mg^{2+} in the LDH structure. After mineralization, monolayer nanosheets were stacked and transformed into multilayer NiMgAl-LDH (Figure S18a), exhibiting the (*00l*) diffraction peaks attributed to the multilayer LDHs (Figure S18b). The apparent lower Ni^{2+} removal capacity of u-MgAl-LDH over the timescale of the experiment is mainly due to the significantly reduced mobility of the divalent ions through the multilayered LDH layers in the ordered staked platelets in u-MgAl-LDH. The mechanism for Cd^{2+} capture is supposed to be similar to Ni^{2+} in which isomorphous substitution of Mg^{2+} for Cd^{2+} ions (Figure S19) is also reported.(Kong et al., 2021)

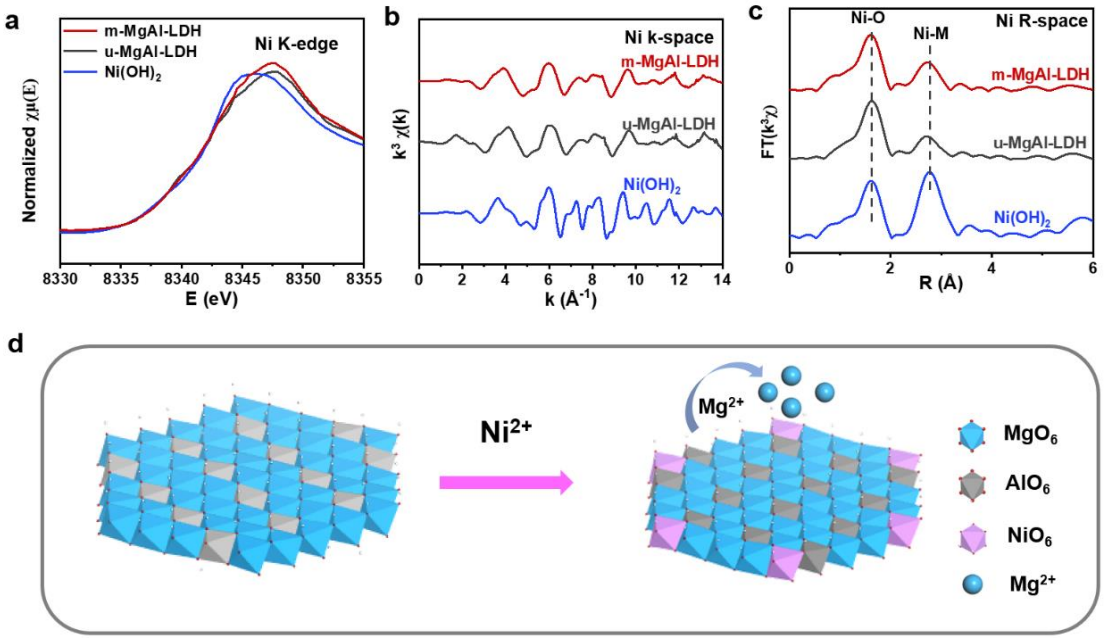

Figure 3. (a) Ni K-edge XANES spectra of m-MgAl-LDH and u-MgAl-LDH after capture and $Ni(OH)_2$, respectively; (b) oscillation function $k^3\chi(k)$ of the K-edge for Ni in the EXAFS of m-MgAl-LDH, u-MgAl-LDH after Ni^{2+} capture and $Ni(OH)_2$, respectively; (c) magnitude of k^3-weighted FT of the Ni K-edge EXAFS spectra; (d) illustration of the MgAl-LDH after adsorbing Ni^{2+} and some of the Mg atoms have been replaced by Ni.

To investigate the possible occupation sites for the Cu^{2+} of the MgAl-LDH structure with different thicknesses, both Cu K-edge XANES and EXAFS X-ray absorption experiments were performed on the samples after Cu^{2+} capture m-MgAl-LDH and u-MgAl-LDH. As shown in Figure 4a, Cu is in the divalent oxidation state in both m-MgAl-LDH and u-MgAl-LDH. In the Cu K-edge EXAFS, the k-space data show extended periods and lower amplitude (Figure 4b). Only Cu-O shell was observed for both m-MgAl-LDH and u-MgAl-LDH

after Cu capture. The absence of the Cu-M shell (around 2.8 Å) suggests that Cu^{2+} is not inserted into the metal hydroxide layers of LDH but is mainly located on the surface of LDH (Figure 4c).(Wang et al., 2019) Due to the strong Jahn-Teller effect in Cu^{2+}, tetrahedral CuO_4 is likely located on the surface of these LDHs. Best fits for the Cu K-edge EXAFS data for m-MgAl-LDH were obtained using a model composed of tetrahedral CuO_4 (Figure S20, Table S7).

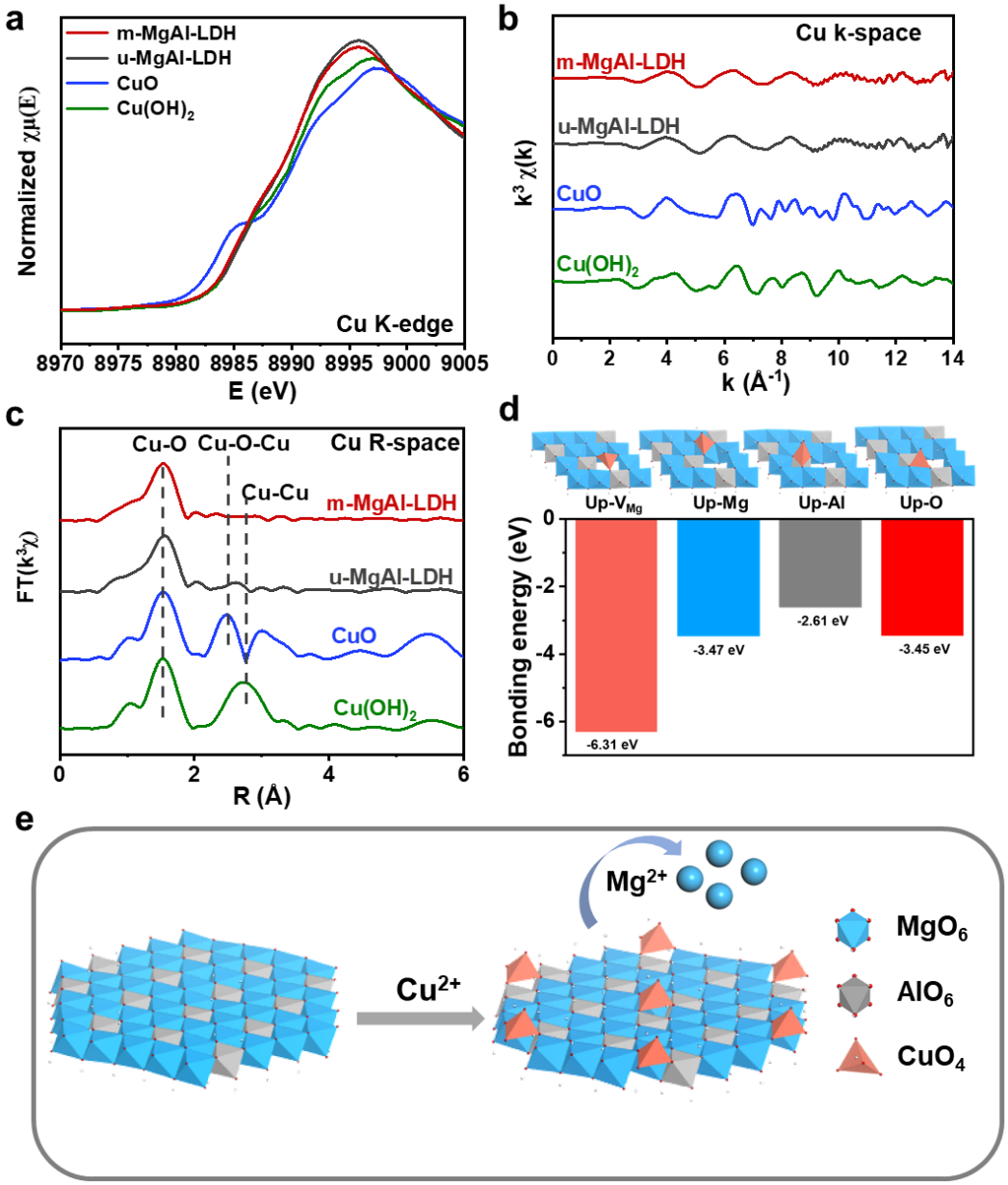

Figure 4. (a) Cu K-edge XANES spectra for m-MgAl-LDH, u-MgAl-LDH, CuO and $Cu(OH)_2$, respectively, (b) oscillation function $k^3\chi(k)$ from the Cu K-edge

EXAFS for m-MgAl-LDH, u-MgAl-LDH after Cu^{2+} removal, CuO and $Cu(OH)_2$, respectively, (c) magnitude of k^3-weighted FT of the Cu K-edge EXAFS spectra, (d) schematic illustration of CuO_4 in the vacancies, and corresponding bonding energy of Up-V_{Mg}, Up-Mg, Up-Al and Up-O, respectively, (e) illustration of the mineralization process for Cu^{2+} ions onto vacancies in m-MgAl-LDH.

Density functional theory (DFT) calculations were employed to understand the possible surface adsorption sites for Cu^{2+} on m-MgAl-LDH. Four models were used: tetrahedral CuO_4 anchored on Mg vacancies, the surface of MgO_6 octahedron, the surface of AlO_6 octahedron, and top site of O atom (denoted as Up-V_{Mg}, Up-Mg, Up-Al, and Up-O, respectively, Figure S21). The above four models were used as stimulation models for the removal sites in m-MgAl-LDH (Figure 4d). The results of the bonding energy of tetrahedral Cu with three O atoms onto the host layers give binding energy of -6.31, -3.47, -2.61 and -3.45 eV for Up-V_{Mg}, Up-Mg, Up-Al and Up-O models, respectively, which suggests that the tetrahedral CuO_4 is thermodynamically favorable located on the surface of LDH, and possibly anchored on the top site of Mg vacancies. This leads to Cu ions being uniformly dispersed on the surface of LDH (Figure 4e). Furthermore, after 180 minutes (Figure S22), more Mg^{2+} was released into solution from m-MgAl-LDH compared to u-MgAl-LDH, and no release of Al^{3+} into the liquid phase could be detected. The leaching of Mg^{2+} from the LDH will result in Mg vacancies, which may provide the sites for further Cu^{2+} sorption. In order to better understand the adsorption site of Cu, we further compared the bonding

energy of two models of Cu locating on Mg vacancies (Up-V_{Mg}) and Cu locating into Mg vacancy (In-V_{Mg}). As shown in Figure S23, the bonding energy for Up-V_{Mg} was -6.31 eV while for In-V_{Mg} was 1.03 eV, which meant that it was a more thermodynamic favourable site for Cu to be located onto the surface of LDHs forming CuO_4, providing a stable mineralization structure. The bonding energy of the second and third Cu^{2+} ions on the same Mg vacancy after the removal of the first Cu^{2+} ion were simulated and calculated (Figure S24). The bonding energy of the second and third Cu^{2+} ion is much lower than that of the first Cu^{2+} ion, which indicates that the Cu^{2+} ions preferentially adsorb on the Mg vacancy with high dispersion when the Mg vacancies are sufficient or the Cu^{2+} ions concentration is low (such as 100 ppm we chose). Such adsorption sites can offer a very low energetic barrier process indicated the Cu^{2+} adsorption sites are on the surface of the LDH. A similar Cu^{2+} uptake capacity for both m-MgAl-LDH and u-MgAl-LDH may arise as both samples can provide enough top-sites for Cu^{2+} to be anchored.

3.4 Reutilization of mineralized products

After clarifying the mineralized mechanism of m-MgAl-LDH on heavy metals, we then studied the application value of mineralized products (ie. NiMgAl-LDH and CuMgAl-LDH after mineralization of Ni and Cu ions over m-MgAl-LDH, respectively). We first explored the application potential of NiMgAl-LDH (that is the mineralized m-MgAl-LDH) compared with the unmineralized m-MgAl-LDH in photocatalytic reduction of CO_2 (CO_2PR). As shown in Figure 5a, compared with m-MgAl-LDH, NiMgAl-LDH showed wider absorption in the visible light region, which can promote light utilization and photocatalytic reactions. In Figure 5b and 5c, we can see that NiMgAl-LDH had

a much higher selectivity of CO and CH_4 than MgAl-LDH from CO_2 reduction. The selectivity of valuable CO was increased from 4.55% of m-MgAl-LDH to 54.62% of NiMgAl-LDH, while that of H_2 decreased from 95.45% of m-MgAl-LDH to 38.93% of NiMgAl-LDH. As NiMgAl-LDH was used as catalyst, CH_4 was present in the product even at wavelength > 500 nm (Figure S25a and S25b), which was attributed to the introduction of Ni active sites.(Hao et al., 2020; Tan et al., 2019; Wu et al., 2021) Excitingly, NiMgAl-LDH still maintained good catalytic activity under the irradiation of light with wavelength > 600 nm and the productivity of CO can reach 0.12 $\mu mol \cdot h^{-1}$ with the assistant of photosensitizer. In the absence of CO_2 (Figure S25c), CO cannot be produced with only trace amounts of H_2, suggesting that CO was converted from CO_2. The comparison experiment showed that there was H_2 without adding NiMgAl-LDH, indicating that $Ru(bpy)_3Cl_2$ $6H_2O$ can carry out hydrogen evolution reaction. The NiMgAl-LDH photocatalyst also had excellent stability and can be recycled for at least 4 times without significant performance degradation (Figure S25d). In addition, NiMgAl-LDH showed lower photoluminescence intensities than m-MgAl-LDH (Figure 5d), indicating that NiMgAl-LDH can better inhibit the recombination of photogenerated electrons and holes and transfer more electrons to its surface, explaining the efficient photocatalytic CO_2 reaction.

Next, we investigated the application prospect of other mineralized products, ie. CuMgAl-LDH in environmental remediation. For dye adsorption experiments, CuMgAl-LDH exhibited excellent dye adsorption ability, effectively removing Congo Red and Evans Blue with removal efficiency greater than 99% and 91% (Figure 5e), respectively. By interacting with the positively

charged sheets of CuMgAl-LDH, the dye anions can be rapidly adsorbed to the surface of CuMgAl-LDH, and the contaminated water can be rapidly decolourized and purified (Figure 5f). CuMgAl-LDH also displayed admirable anion adsorption ability, removing phosphate ion (20 ppm) and toxic arsenate ion (100 ppm) with removal efficiency over 80% (Figure 5g, h). The acid anions can be rapidly adsorbed in the interlayer region of CuMgAl-LDH by connecting with the positively charged sheets of CuMgAl-LDH. These results demonstrate that LDH-derived mineralized products can efficiently convert CO_2 into fuel through photocatalysis and quickly remove organic dyes and acid anions from sewage, providing an interesting solution to the energy crisis and environmental pollution.

From the above results, it can be concluded that the obtained monolayer LDH nanosheets provide abundant active sites for the efficient mineralization of Ni^{2+}, Cd^{2+} and Cu^{2+} ions. According to Table S8, m-MgAl-LDH exhibited top-level mineralization performance in the three aspects of capacity, removal efficiency, and the low equilibrium limit, and the mineralized products also show potential application in photocatalytic reduction of CO_2 and environmental remediation.

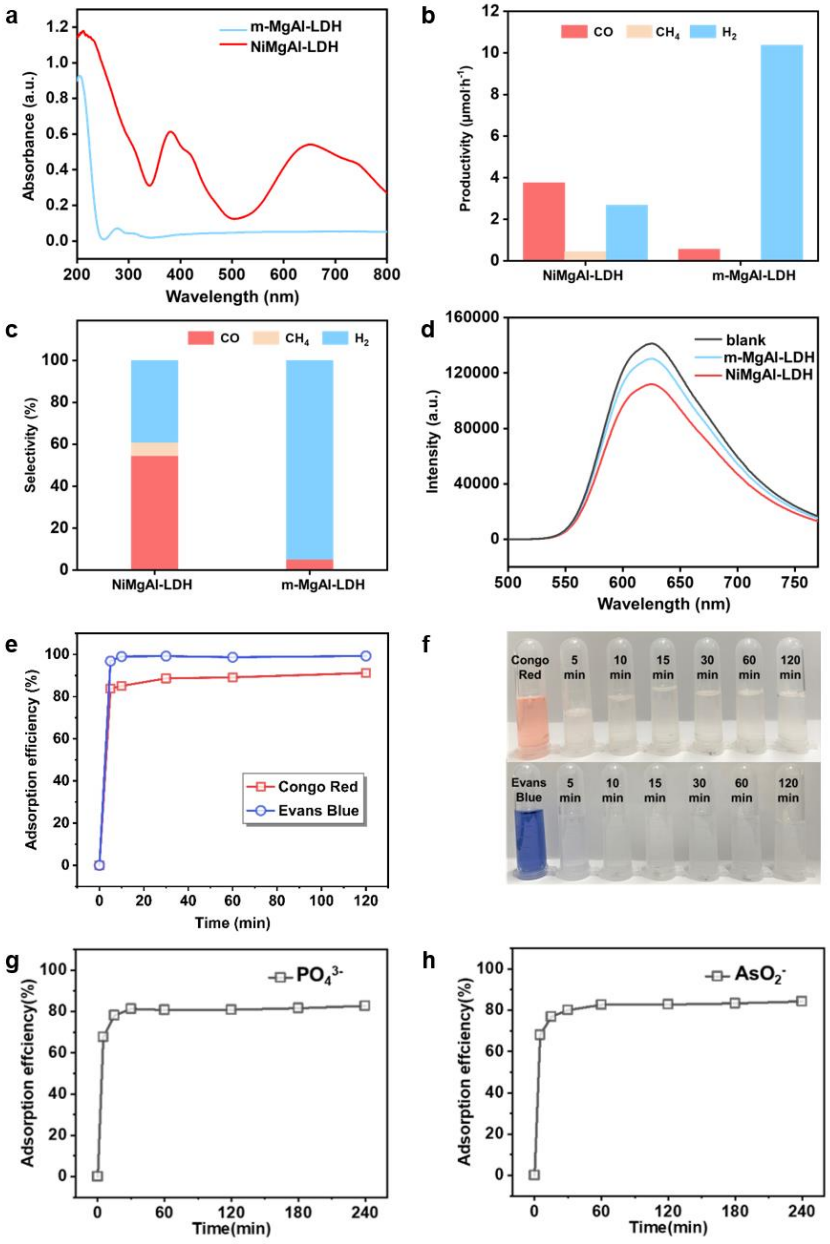

Figure 5. (a) UV-visible spectra of the mineralization product NiMgAl-LDH and m-MgAl-LDH; (b) Yield and (c) Selectivity of CH_4, CO, and H_2 in CO_2PR on NiMgAl-LDH and m-MgAl-LDH under irradiation above 400 nm; (d) Room-temperature photoluminescence spectra of NiMgAl-LDH and m-MgAl-LDH; Blank stands for the control group with only $Ru(bpy)_3Cl_2 \cdot 6H_2O$ and H_2O/MeCH/TEOA; (e) Adsorption efficiency of CuMgAl-LDH for dyes and (f)

appearance of the adsorption process; Adsorption efficiency of CuMgAl-LDH for (g) PO_4^{3-} and (h) AsO_2^-.

4. Conclusion

We reported a convenient, scalable synthesis of monolayer m-MgAl-LDH. This material exhibited outstandingly rapid mineralization of Ni^{2+}, Cd^{2+}, and Cu^{2+} from aqueous solution. In particular, m-MgAl-LDH can capture greater than 99% of the Cu^{2+}, Ni^{2+} and Cd^{2+} at 1 ppm concentrations to produce aqueous solutions meeting safe levels. The platelet dispersion of the MgAl-LDH is key to achieving this rapid removal performance with high efficiency. XAFS data provides clear insights on how these cations are mineralized into the LDH nanosheets. Specifically, Ni^{2+} and Cd^{2+} ions underwent isomorphous substitution, while Cu^{2+} ions were shown to be located on the surface of LDH nanosheets. After capturing heavy metals, the mineralized products can be further used for photocatalytic reduction of CO_2 and anions adsorption in sewage, approaching the goal of sustainable development by using waste to treat waste. This work here has expended the application of monolayer LDHs to mineralize heavy metal pollutions for the application in photocatalysis and beyond.

Author Contributions

Tianyi Lai: Investigation, Writing - original draft. Wenbo Xiong and Huijuan Wang: Investigation, Data curation, Formal analysis. Jikang Wang: Editing and DFT analysis. Mufei Yang: Investigation, Data curation, Formal analysis. Tian Li: Investigation, Data curation, Formal analysis. Xianggui Kong and Xiaoxin Zou: Investigation. Dermot O'Hare: Data curation, Validation. Yufei Zhao: Conceptulization, Administration,

Formal analysis, Writing - review & editing. Yu-Fei Song: Conceptulization, Administration, Formal analysis, Writing - review & editing.

Conflicts of interest

There are no conflicts to declare.

Acknowledgements

This work was supported by the National Natural Science Foundation of China (21922801, 22090032, 22011530162), the Transformation of Scientific and Technological Achievements in Qinghai Province (2021-GX-172), the Beijing Natural Science Foundation (2202036). The XAFS and XES experiments were conducted in 1W1B and 1W2B beamline of the Beijing Synchrotron Radiation Facility (BSRF). The plating wastewater was provided by AVIC Beijing Keeven Aviation Instrument Co., Ltd.

References

2010. Guidelines for drinking-water quality, 4th edition, incorporating the 1st addendum. World Health Organization.

Bai, S., Li, T., Wang, H., Tan, L., Zhao, Y., Song, Y.-F., 2021. Scale-up synthesis of monolayer layered double hydroxide nanosheets via separate nucleation and aging steps method for efficient CO_2 photoreduction. Chemical Engineering Journal 419, 129390.

Bilal, M., Shah, J.A., Ashfaq, T., Gardazi, S.M., Tahir, A.A., Pervez, A., Haroon, H., Mahmood, Q., 2013. Waste biomass adsorbents for copper removal from industrial wastewater--a review. Journal of Hazardous Materials 263 322-333.

Chen, C., Tao, L., Du, S., Chen, W., Wang, Y., Zou, Y., Wang, S., 2020. Advanced Exfoliation Strategies for Layered Double Hydroxides and Applications in Energy Conversion and Storage. Advanced Functional Materials 30, 1909832.

Chi, H., Dong, J., Li, T., Bai, S., Tan, L., Wang, J., Shen, T., Liu, G., Liu, L., Sun, L., Zhao, Y., Song, Y.-F., 2020. Scaled-up synthesis of defect-rich layered double hydroxide monolayers without organic species for efficient oxygen evolution reaction. Green Energy & Environment.

Egene, C.E., Van Poucke, R., Ok, Y.S., Meers, E., Tack, F.M.G., 2018. Impact of organic amendments (biochar, compost and peat) on Cd and Zn mobility and solubility in contaminated soil of the Campine region after three years. Science of the Total Environment 626, 195-202.

Evans, D.G., Duan, X., 2006. Preparation of layered double hydroxides and their applications as additives in polymers, as precursors to magnetic materials and in biology and medicine. Chemical Communications 5, 485-496.

Farrukh, A., Akram, A., Ghaffar, A., Hanif, S., Hamid, A., Duran, H., Yameen, B., 2013. Design of polymer-brush-grafted magnetic nanoparticles for highly efficient water remediation. ACS Applied Materials & Interfaces 5, 3784-3793.
Feizi, M., Jalali, M., Antoniadis, V., Shaheen, S.M., Ok, Y.S., Rinklebe, J., 2019. Geo- and nano-materials affect the mono-metal and competitive sorption of Cd, Cu, Ni, and Zn in a sewage sludge-treated alkaline soil. Journal of Hazardous Materials 379, 120567.
Feng, Y., Li, D., Wang, Y., Evans, D.G., Duan, X., 2006. Synthesis and characterization of a UV absorbent-intercalated Zn–Al layered double hydroxide. Polymer Degradation and Stability 91, 789-794.
Funnell, N.P., Wang, Q., Connor, L., Tucker, M.G., O'Hare, D., Goodwin, A.L., 2014. Structural characterization of a layered double hydroxide nanosheet. Nanoscale 6, 8032-8036.
Gore, C.T., Omwoma, S., Chen, W., Song, Y.-F., 2016. Interweaved LDH/PAN nanocomposite films: Application in the design of effective hexavalent chromium adsorption technology. Chemical Engineering Journal 284, 794-801.
Guan, W., Zhang, B., Tian, S., Zhao, X., 2018. The synergism between electro-Fenton and electrocoagulation process to remove Cu-EDTA. Applied Catalysis B: Environmental 227, 252-257.
Guo, Y., Li, X., Liang, L., Lin, Z., Su, X., Zhang, W., 2021. Immobilization of cadmium in contaminated soils using sulfidated nanoscale zero-valent iron: Effectiveness and remediation mechanism. Journal of Hazardous Materials 420, 126605.
Hao, X., Tan, L., Xu, Y., Wang, Z., Wang, X., Bai, S., Ning, C., Zhao, J., Zhao, Y., Song, Y.-F., 2020. Engineering Active Ni Sites in Ternary Layered Double Hydroxide Nanosheets for a Highly Selective Photoreduction of CO_2 to CH_4 under Irradiation above 500 nm. Industrial & Engineering Chemistry Research 59, 3008-3015.
Haoyuan, C., Jikang, W., Huijuan, W., Shaoquan, L., Mufei, Y., Sha, B., Changjuan, L., Xiaoliang, S., Yufei, Z., Yu-Fei, S., 2021. Super-Stable Mineralization of Ni2+ Ions from Wastewater using CaFe Layered Double Hydroxide. ADVANCED FUNCTIONAL MATERIALS.
He, L., Liu, S., Chen, L., Dai, X., Li, J., Zhang, M., Ma, F., Zhang, C., Yang, Z., Zhou, R., Chai, Z., Wang, S., 2019. Mechanism unravelling for ultrafast and selective 99TcO4− uptake by a radiation-resistant cationic covalent organic framework: a combined radiological experiment and molecular dynamics simulation study. Chemical Science 10, 4293-4305.
He, S., Chen, C., Chen, G., Chen, F., Dai, J., Song, J., Jiang, F., Jia, C., Xie, H., Yao, Y., Hitz, E., Chen, G., Mi, R., Jiao, M., Das, S., Hu, L., 2020. High-Performance, Scalable Wood-Based Filtration Device with a Reversed-Tree Design. CHEMISTRY OF MATERIALS 32, 1887-1895.
Hoang, M.T., Pham, T.D., Verheyen, D., Nguyen, M.K., Pham, T.T., Zhu, J., Van der Bruggen, B., 2020. Fabrication of thin film nanocomposite nanofiltration membrane incorporated with cellulose nanocrystals for removal of Cu(II) and Pb(II). CHEMICAL ENGINEERING SCIENCE 228, 115998.
Hu, L., Wei, Z., Yu, F., Yuan, H., Liu, M., Wang, G., Peng, B., Dai, B., Ma, J., 2019. Defective ZnS nanoparticles anchored in situ on N-doped carbon as a superior oxygen reduction reaction catalyst. J. Energy Chem. 39, 152-159.
Jin, Z., Li, Y., Ma, Q., 2020. CoAl LDH@Ni-MOF-74 S-Scheme Heterojunction for Efficient Hydrogen Evolution. Transactions of Tianjin University.
Kim, N., Gu, T.-H., Shin, D., Jin, X., Shin, H., Kim, M.G., Kim, H., Hwang, S.-J., 2021. Lattice Engineering to Simultaneously Control the Defect/Stacking Structures of Layered Double Hydroxide Nanosheets to Optimize Their Energy Functionalities. ACS Nano 15, 8306-8318.
Kong, X., Ge, R., Liu, T., Xu, S., Hao, P., Zhao, X., Li, Z., Lei, X., Duan, H., 2021. Super-stable mineralization of cadmium by calcium-aluminum layered double hydroxide and its large-scale application in agriculture soil remediation. CHEMICAL ENGINEERING JOURNAL 407, 127178.
Krstić, V., Urošević, T., Pešovski, B., 2018. A review on adsorbents for treatment of water and wastewaters containing copper ions. CHEMICAL ENGINEERING SCIENCE 192, 273-287.
Kuai, C., Zhang, Y., Wu, D., Sokaras, D., Mu, L., Spence, S., Nordlund, D., Lin, F., Du, X.-W., 2019. Fully Oxidized Ni-Fe Layered Double Hydroxide with 100% Exposed Active Sites for Catalyzing Oxygen Evolution Reaction. ACS Catalysis 9, 6027-6032.
Lam, B., Déon, S., Morin-Crini, N., Crini, G., Fievet, P., 2018. Polymer-enhanced ultrafiltration for heavy metal removal: Influence of chitosan and carboxymethyl cellulose on filtration performances. Journal of Cleaner Production 171, 927-933.
Lan, M., Fan, G., Wang, Y., Yang, L., Li, F., 2014. Synthesis of highly dispersed boron-promoted nickel nanocatalysts and significantly enhanced catalytic performance in hydrodechlorination of chlorobenzene. Journal of Materials Chemistry A 2, 14682-14699.
Li, J., Fan, Q., Wu, Y., Wang, X., Chen, C., Tang, Z., Wang, X., 2016. Magnetic polydopamine decorated with Mg–Al LDH nanoflakes as a novel bio-based adsorbent for simultaneous removal of potentially toxic metals and anionic dyes. Journal of Materials Chemistry A 4, 1737-1746.

Li, M., Mu, Y., Shang, H., Mao, C., Cao, S., Ai, Z., Zhang, L., 2020. Phosphate modification enables high efficiency and electron selectivity of nZVI toward Cr(VI) removal. Applied Catalysis B: Environmental 263, 118364.
Liu, Y., Gao, Y., Zhang, Z., Wang, Q., 2021. Preparation of ammonium polyphosphate and dye co-intercalated LDH/polypropylene composites with enhanced flame retardant and UV resistance properties. Chemosphere 277, 130370.
Ma, L., Islam, S.M., Xiao, C., Zhao, J., Liu, H., Yuan, M., Sun, G., Li, H., Ma, S., Kanatzidis, M.G., 2017. Rapid Simultaneous Removal of Toxic Anions $[HSeO_3]^-$, $[SeO_3]^{2-}$, and $[SeO_4]^{2-}$, and Metals Hg^{2+}, Cu^{2+}, and Cd^{2+} by MoS_4^{2-} Intercalated Layered Double Hydroxide. Journal of the American Chemical Society 139, 12745-12757.
Miao, J., Zhao, X., Zhang, Y.-X., Liu, Z.-H., 2021. Feasible synthesis of hierarchical porous MgAl-borate LDHs functionalized Fe_3O_4@SiO_2 magnetic microspheres with excellent adsorption performance toward congo red and Cr(VI) pollutants. Journal of Alloys and Compounds 861, 157974.
Sajid, M., Basheer, C., 2016. Layered double hydroxides: Emerging sorbent materials for analytical extractions. TrAC Trends in Analytical Chemistry 75, 174-182.
Shan, R.R., Yan, L.G., Yang, K., Hao, Y.F., Du, B., 2015. Adsorption of Cd(II) by Mg-Al-CO_3- and magnetic Fe_3O_4/Mg-Al-CO_3-layered double hydroxides: Kinetic, isothermal, thermodynamic and mechanistic studies. Journal of Hazardous Materials 299, 42-49.
Shi, M., Zhao, Z., Song, Y., Xu, M., Li, J., Yao, L., 2020. A novel heat-treated humic acid/MgAl-layered double hydroxide composite for efficient removal of cadmium: Fabrication, performance and mechanisms. Applied Clay Science 187, 105482.
Song, F., Hu, X., 2014. Exfoliation of layered double hydroxides for enhanced oxygen evolution catalysis. Nature Communication 5, 4477-4485.
Szczepaniak, G., Piątkowski, J., Nogaś, W., Lorandi, F., Yerneni, S.S., Fantin, M., Ruszczyńska, A., Enciso, A.E., Bulska, E., Grela, K., Matyjaszewski, K., 2020. An isocyanide ligand for the rapid quenching and efficient removal of copper residues after Cu/TEMPO-catalyzed aerobic alcohol oxidation and atom transfer radical polymerization. Chemical Science 11, 4251-4262.
Tan, L., Xu, S.-M., Wang, Z., Xu, Y., Wang, X., Hao, X., Bai, S., Ning, C., Wang, Y., Zhang, W., Jo, Y.K., Hwang, S.-J., Cao, X., Zheng, X., Yan, H., Zhao, Y., Duan, H., Song, Y.-F., 2019. Highly Selective Photoreduction of CO2 with Suppressing H-2 Evolution over Monolayer Layered Double Hydroxide under Irradiation above 600 nm. Angewandte Chemie International Edition 58, 11860-11867.
Vital, B., Bartacek, J., Ortega-Bravo, J.C., Jeison, D., 2018. Treatment of acid mine drainage by forward osmosis: Heavy metal rejection and reverse flux of draw solution constituents. Chemical Engineering Journal 332, 85-91.
Wang, J., Zhang, W., Yue, X., Yang, Q., Liu, F., Wang, Y., Zhang, D., Li, Z., Wang, J., 2016. One-pot synthesis of multifunctional magnetic ferrite–MoS_2–carbon dot nanohybrid adsorbent for efficient Pb(ii) removal. Journal of Materials Chemistry A 4, 3893-3900.
Wang, L., Xu, X., Evans, D.G., Duan, X., Li, D., 2010. Synthesis and selective IR absorption properties of iminodiacetic-acid intercalated MgAl-layered double hydroxide. Journal of Solid State Chemistry 183, 1114-1119.
Wang, Q., O'Hare, D., 2012. Recent advances in the synthesis and application of layered double hydroxide (LDH) nanosheets. Chemical Review 112, 4124-4155.
Wang, Q., O'Hare, D., 2013. Large-scale synthesis of highly dispersed layered double hydroxide powders containing delaminated single layer nanosheets. Chemical Communications 49, 6301-6303.
Wang, X., Liang, Y., An, W., Hu, J., Zhu, Y., Cui, W., 2017a. Removal of chromium (VI) by a self-regenerating and metal free g-C_3N_4/graphene hydrogel system via the synergy of adsorption and photocatalysis under visible light. Applied Catalysis B: Environmental 219, 53-62.
Wang, Y., Xie, C., Zhang, Z., Liu, D., Chen, R., Wang, S., 2018. In Situ Exfoliated, N-Doped, and Edge-Rich Ultrathin Layered Double Hydroxides Nanosheets for Oxygen Evolution Reaction. Advanced Functional Materials 28, 1703363.
Wang, Y., Zhang, Y., Liu, Z., Xie, C., Feng, S., Liu, D., Shao, M., Wang, S., 2017b. Layered Double Hydroxide Nanosheets with Multiple Vacancies Obtained by Dry Exfoliation as Highly Efficient Oxygen Evolution Electrocatalysts. Angewandte Chemie International Edition 56, 5867-5871.
Wang, Z., Xu, S.M., Xu, Y., Tan, L., Wang, X., Zhao, Y., Duan, H., Song, Y.F., 2019. Single Ru atoms with precise coordination on a monolayer layered double hydroxide for efficient electrooxidation catalysis. Chemical Science 10, 378-384.
Wu, D., Zhao, X., Huang, Y., Lai, J., Li, H., Yang, J., Tian, C., He, P., Huang, Q., Tang, X., 2021. Lead-Free Perovskite Cs2AgBiX6 Nanocrystals with a Band Gap Funnel Structure for Photocatalytic CO2

Reduction under Visible Light. CHEMISTRY OF MATERIALS 33, 4971-4976.
Xu, S., Zhang, L., Lin, Y., Li, R., Zhang, F., 2012. Layered double hydroxides used as flame retardant for engineering plastic acrylonitrile–butadiene–styrene (ABS). Journal of Physics and Chemistry of Solids 73, 1514-1517.
Xu, Z., Shan, C., Xie, B., Liu, Y., Pan, B., 2017. Decomplexation of Cu(II)-EDTA by UV/persulfate and UV/H_2O_2: Efficiency and mechanism. Applied Catalysis B: Environmental 200, 439-447.
Yu, C., Shao, Z., Hou, H., 2017a. A functionalized metal–organic framework decorated with O− groups showing excellent performance for lead(ii) removal from aqueous solution. Chemical Science 8, 7611-7619.
Yu, J., Martin, B.R., Clearfield, A., Luo, Z., Sun, L., 2015. One-step direct synthesis of layered double hydroxide single-layer nanosheets. Nanoscale 7, 9448-9451.
Yu, J., Wang, Q., O'Hare, D., Sun, L., 2017b. Preparation of two dimensional layered double hydroxide nanosheets and their applications. Chemical Society Reviews 46, 5950-5974.
Zhang, L., Guo, D., Tantai, X., Jiang, B., Sun, Y., Yang, N., 2020. Synthesis of Three-Dimensional Hierarchical Flower-Like Mg–Al Layered Double Hydroxides with Excellent Adsorption Performance for Organic Anionic Dyes. Transactions of Tianjin University.
Zhao, K., Li, X., Su, D., 2020. High-Entropy Alloy Nanocatalysts for Electrocatalysis. Acta Physico Chimica Sinica 37, 2012052.
Zhao, Y., Jia, X., Chen, G., Shang, L., Waterhouse, G.I., Wu, L.Z., Tung, C.H., O'Hare, D., Zhang, T., 2016. Ultrafine NiO Nanosheets Stabilized by TiO_2 from Monolayer NiTi-LDH Precursors: An Active Water Oxidation Electrocatalyst. Journal of the American Chemical Society 138, 6517-6524.
Zhou, Q., Liao, B., Lin, L., Qiu, W., Song, Z., 2018. Adsorption of Cu(II) and Cd(II) from aqueous solutions by ferromanganese binary oxide-biochar composites. Science of the Total Environment 615, 115-122.